Nanoscale

Improvement in Quantum Yield by Suppression of Trions in Room Temperature Synthesized CsPbBr3 Perovskite Quantum Dots for Backlight Display

Journal:	*Nanoscale*
Manuscript ID	NR-ART-10-2019-009056.R1
Article Type:	Paper
Date Submitted by the Author:	29-Nov-2019

Complete List of Authors:	Dave, Kashyap; National Taiwan University, Department of Chemistry Bao, Zhen; National Taiwan University, Department of Chemistry Nakahara, Satoshi ; Kyoto University - Uji Campus, Institute for Chemical Research Ohara, Keiichi ; Kyoto University - Uji Campus, Institute for Chemical Research Masada, Sojiro ; Kyoto University - Uji Campus, Institute for Chemical Research Tahara, Hirokazu; Kyoto University - Uji Campus, Institute for Chemical Research Kanemitsu, Yoshihiko; Kyoto University - Uji Campus, Institute for Chemical Research Liu, Ru-Shi; National Taiwan University, Department of Chemistry

ARTICLE

Improvement in Quantum Yield by Suppression of Trions in Room Temperature Synthesized $CsPbBr_3$ Perovskite Quantum Dots for Backlight Display

Kashyap Dave,[a,b,] Zhen Bao,[a] Satoshi Nakahara,[c] Keiichi Ohara,[c] Sojiro Masada,[c] Hirokazu Tahara,[c] Yoshihiko Kanemitsu[c]* and Ru-Shi Liu[a,d]*

Received 00th January 20xx,
Accepted 00th January 20xx

DOI: 10.1039/x0xx00000x

Surface defects and synthesis methods play important roles on the photoluminescence quantum yield (PLQY), stability, and device performance of lead halide perovskite quantum dots (PQDs). In this study, we report a quadruple-ligand tri-n-octylphosphine, didodecyldimethylammonium bromide, tetraoctylammonium bromide, and oleic acid assisted room-temperature method for synthesizing $CsPbBr_3$ QDs (RT-$CsPbBr_3$) with absolute PLQY of 83%. X-ray photoelectron spectroscopy confirms the high completeness of Pb–Br octahedron through the absence of lead ions and high bromide ions on the surface of RT-$CsPbBr_3$ QDs. The exciton dynamics of RT-$CsPbBr_3$ QDs are studied by using femtosecond transient absorption, time-resolved PL, and single-dot spectroscopy, which provide strong evidence of suppression of trion formation compared with the hot injection-synthesized $CsPbBr_3$ (HI-$CsPbBr_3$) QDs. The white light-emitting diode (LED) is fabricated with RT-$CsPbBr_3$ PQDs and K_2SiF_6: Mn^{4+} phosphor for backlight applications achieved a wide color gamut of 124% National Television System Committee (NTSC) standard.

Introduction

Perovskite quantum dots (PQDs) have received great attention from numerous researchers because of their strong photoluminescence (PL), narrow full width at half maxima (FWHM), high defect tolerance and tunable wavelength.[1, 2] These advantages succeed it more suitable candidate for optoelectronic applications such as photovoltaic cell,[3] light-emitting diode,[4, 5] photodetectors,[6, 7] and lasing.[8] Several solution-processing methods, such as hot injection (HI),[9] ligand-assisted re-precipitation (LARP),[10] and micromechanical method,[11] have been reported to produce colloidal PQDs. HI is mostly used among these methods. However, this method needs high temperature, inert gas, vacuum environment, and controlled injection of cesium precursor, thereby making it difficult to scale up at industrial applications. In addition, researchers used post-synthetic treatment,[12] ligand-assisted assembly,[13, 14] coating[15, 16] and cations doping.[17, 18] to improve the quantum yield and stability. For the replacement of the HI method, a number of room temperature (RT) methods have been reported, such as recrystallization,[19] emulsions,[20]and triple-ligand-assisted method.[13] PQDs produced via these methods show high PL performance which makes them more suitable for commercialization. Li *et al.*[19] first reported a super-saturation recrystallization method for synthesizing $CsPbX_3$ (X = Cl, Br, and I) QDs. After that, Kim *et al.*[20] reported an emulsion method, where perovskite precursors were mixed in dimethylformamide and dropped into hexane containing oleic acid and amine, which further crystallize into quantum dots after adding tert-butanol as a demulsifier. Wei *et al.*[21] described the homogenous synthesis of $CsPbBr_3$ at room temperature but applied 120 °C to prepare cesium oleate, and TOAB to dissolve $PbBr_2$ in toluene. Then Song *et al.*[13] reported the triple ligand-assisted assembly of $CsPbBr_3$, which used stirring to dissolve cesium carbonate into octanoic acid. However, we found it is difficult to prepare cesium oleate precursor at room temperature. To overcome this issue, we proposed ultra-sonication for dispersing cesium carbonate into oleic acids and used additional tri-n-octylphosphine (TOP) ligand with TOAB to help $PbBr_2$ to dissolve in toluene.

In addition to synthesis methods, surface defects play a crucial role to affect the photoluminescence quantum yield (PLQY) of PQDs, which leads to trap the charge carriers and consequence reduce PLQY.[10] These surface defects in lead halide perovskite are origin from the presence of Pb ions and low halide density on the surface of PQDs.[22] While these surface defects could be passivated through the ligands or surface treatment to achieve high PLQY.[23] Ahmed *et al.*[12] found that the removal of the excess Pb ions after surface treatment of tetrafluoroborate on $CsPbX_3$ enhanced PLQY. Koscher *et al.*[24] reported that thiocyanate

[a.] *Department of Chemistry and Advanced Research Center of Green Materials Science and Technology, National Taiwan University, Taipei 106, Taiwan.*
[b.] *Nanoscience and Technology Program, Taiwan International Graduate Program, Academia Sinica and National Taiwan University, Taipei 115, Taiwan.*
[c.] *Institute for Chemical Research, Kyoto University, Uji, Kyoto 611-0011, Japan.*
[d.] *Department of Mechanical Engineering and Graduate Institute of Manufacturing Technology, National Taipei University of Technology, Taipei 106, Taiwan.*
*Email: rsliu@ntu.edu.tw. (R.S. Liu)
*Email: kanemitu@scl.kyoto-u.ac.jp. (Y. Kanemitsu)
Electronic Supplementary Information (ESI) available: [details of any supplementary information available should be included here]. See DOI: 10.1039/x0xx00000x

treatment removes the excess amount of lead from all $CsPbX_3$ QDs, thereby improving quantum yield. On another side, Nakahara *et al*.[25] carried out a transient absorption (TA) study on thiocyanate treated of $CsPbBr_3$ and found trion (charged exciton) formation was suppressed compared with pristine PQDs, which is the mechanism of PLQY enhancement. The formation and suppression of trions are closely related to the surface treatment of PQDs and which affect the PLQY of PQDs.[26]

Here, we report a ligand-assisted RT method for synthesis $CsPbBr_3$ with satisfactory absolute PLQY of 83% and only reduce to 81% after 112 days. X-ray diffraction (XRD) confirmed the cubic phase of PQDs synthesized in both methods. X-ray photoelectron spectroscopy (XPS) revealed the surface environment of Pb and Br ions. TA spectroscopy, single-dot spectroscopy, and time-resolved PL are performed to study the exciton dynamics in RT-$CsPbBr_3$ and HI-$CsPbBr_3$ QDs. The RT-$CsPbBr_3$ QDs are demonstrated to white light-emitting diodes (LED) fabrication for backlight application.

Experimental section

Reagents: The following chemicals were used without purification: cesium carbonate (Cs_2CO_3, 99.00%), 1- octadecene (ODE, 90.00%), toluene (99.80%), and oleic acid (99.0%) were purchased from Sigma Aldrich; lead bromide ($PbBr_2$, 99.99%), tetraoctylammonium bromide (TOAB, 98.00%), tri-n-octylphosphine (TOP, 90.00%), and silicone resins A and B (OE6631) were purchased from ABCR, Fluka, Alfa Aesar, and Dow Corning, respectively; oleylamine (80.00-90.00%and didodecyldimethylammonium bromide (DDAB, 99.00%%) were purchased from Acros Organics. n-Hexane (95.00%) and acetone (99.5%) purchased from ECHO and Honeywell respectively.

Room temperature synthesis of $CsPbBr_3$: Room temperature (RT) synthesis of $CsPbBr_3$ was carried out as follows: 16.24 mg of Cs_2CO_3 was added into 10 mL of oleic acid and sonicated for 1.5 h to complete dispersion. Simultaneously, 18.35 mg of $PbBr_2$ was mixed in 1 mL of TOP for 1 h at 800 rpm and continually stirred. Subsequently, 10 mL of toluene was added, and the reaction was transformed to 400 rpm to avoid bubbles. Approximately 5.46 mg of TOAB was added to the solution and continually stirred. Afterward, 4.62 mg of DDAB was directly supplemented into the solution after TOAB addition and stirred for 10 min. Thereafter, 1 mL of Cs-oleate was added into the $PbBr_2$-toluene solution, and the color changed to bright green. The reaction lasted for 3 min, and 30 mL of acetone was then added for precipitation. The solution was centrifuged at 10,000 rpm for 6 min and dispersed in 2 mL of hexane, followed by twofold centrifugation at 8000 rpm for 6 min.

Hot injection synthesis of $CsPbBr_3$: Hot injection (HI) was used after certain modifications in the previously reported method10. Approximately 407 mg of Cs_2CO_3 was added into 20 mL of octadecene with 1.25 mL of oleic acid in a three-neck glass container and continually stirred. Thereafter, 276 mg of $PbBr_2$ was added in 20 mL of ODE with 2 mL of oleic acid and 2 mL of oleylamine in a three-neck glass container and continually stirred. Both containers were kept at 120 °C in a vacuum for 1 h, and the $PbBr_2$ temperature was then raised to 180 °C. Subsequently, N_2 was introduced in both containers for 10 min. Afterward, 1.6 mL added into the $PbBr_2$ solution within 5-10 s, and the reaction was cooled down by an ice bath. The solution was then centrifuged at 8000 rpm for 6 min to remove oil. Finally, 2 mL n-hexane was added and centrifuged to obtain the final perovskite quantum dots (PQDs).

Package of LEDs based on RT-$CsPbBr_3$ or HI-$CsPbBr_3$: In this procedure, 0.50 mL RT-$CsPbBr_3$ QDs were added to mortar, and 0.05 mg of resin B was then mixed. Subsequently, 0.025 mg of resin A was added and properly re-mixed. After the bubbles were removed, the mixture was dropped onto a blue-chip and then thermally dried at 150 °C for 2 h in an oven. The optical properties of the RT-$CsPbBr_3$ and HI-$CsPbBr_3$ fabricated devices were determined with an integrating sphere by using an analyzer system (Everfine Photo-EINFO Co., Ltd.). Approximately 0.025 mL of HI-$CsPbBr_3$ was added instead of RT-$CsPbBr_3$. The other process was similar.

Characterizations: The powder X-ray diffractometer was used to determine the crystal structure of RT and HI $CsPbBr_3$ on the glass with a D2 phaser diffractometer from Bruker with Cu Kα radiation (λ = 1.5418 Å). Transmission electron microscopy was performed on the Jeol JEM-1200 EX II high-resolution transmission electron microscope. The FluoroMax-4P TCSPC spectrofluorometer was used to measure the photoluminescence emission at 460 nm excitation. Absorption spectra were collected with a UV/Vis spectrophotometer (Shimadzu UV-700). The absolute quantum yield was measured by using Hamamatsu Quantaurus QY. Fourier-transform infrared spectra measured by Varian 640-IR for both QDs. X-ray photoelectron spectra were obtained from Thermo Scientific, Theta Probe.

Optical Measurements: For the transient absorption (TA) and time-resolved photoluminescence (TRPL) spectroscopies, we used a Yb: KGW-based femtosecond laser system (Pharos, Light Conversion) with an optical parametric amplifier (Orpheus, Light Conversion). The pulse duration and repetition rates were 300 fs and 10 kHz, respectively. The center wavelength of the excitation pulse was tuned to 400 nm. In the TA spectroscopy, in addition to the excitation pump pulse, a white-light probe pulse was generated by focusing a fundamental laser pulse of the Yb: KGW-based laser system into distilled water. The TA spectra were detected by using a spectrometer and a silicon-based array detector. To obtain the generation ratios of excitons, trions, and biexcitons, we performed a fitting analysis of the TA decay curves by using a triple exponential decay function: $A_X e^{-t/\tau_X} + A_{X^*} e^{-t/\tau_{X^*}} + A_{XX} e^{-t/\tau_{XX}}$. Here, the amplitudes and lifetimes correspond to those of the exciton (X), trion (X*), and biexciton (XX) components. From the fitting analysis, the lifetimes were obtained to be $\tau_X = 6.7$ ns, $\tau_{X^*} = 350$ ps, and $\tau_{XX} = 41$ ps for RT-$CsPbBr_3$ and $\tau_X = 5.3$ ns, $\tau_{X^*} = 220$ ps, and $\tau_{XX} = 30$ ps for HI-$CsPbBr_3$. These lifetimes are independent of the excitation fluence, while the amplitudes increase with the excitation fluence as shown in Figures 4(b) and 4(d). In the TRPL spectroscopy, the PL spectra were detected by using a visible streak camera (Hamamatsu

Photonics). We obtained similar generation ratios of excitons, trions, and biexcitons from the TRPL signals.

Single-dot spectroscopy measurements: we performed a single photon counting of the PL signals emitted from single PQDs. We used a supercontinuum light source (WhiteLase, Fianium) and the excitation wavelength was selected to 420 nm by a tunable bandpass filter (SuperChrome, Fianium). The single photons were collected by an oil immersion objective (100×, NA = 1.45). The single photons were analyzed by a Hanbury-Brown Twiss interferometer with two avalanche photodiodes (APDs) (SPD-050-CTE, Micro Photon Devices). The APD signals were recorded by time-correlated single-photon counting boards (SPC-130EM, Becker & Hickl GmbH).

Results and discussion

HI-$CsPbBr_3$ QDs are synthesized through some modification in the previously reported method for comparative study.[17] In the hot injection method, a high temperature (>120 °C) used to dissolve Cs_2CO_3 and $PbBr_2$ in vacuum. Oleic acid and oleylamine are used as surface ligands. On the other side, RT-$CsPbBr_3$ QDs are synthesized using in-situ nucleation in the presence of four ligands: TOP, DDAB, TOAB, and oleic acid. First, the Cs-oleate complex prepared via the ultra-sonication treatment of Cs_2CO_3 in oleic acid. To avoid the use of temperature, first $PbBr_2$ mixed within surfactant TOP and stirrer for 1 h. Consequently, solvent toluene is added, but still $PbBr_2$ not completely dissolve. Further TOAB and DDAB subsequently added which completely dissolve the $PbBr_2$. $CsPbBr_3$ QDs are nucleated after adding Cs-oleate into the ligand-containing $PbBr_2$ precursor as shown in **Scheme**. The complete synthesis process for both elaborated in the experimental section.

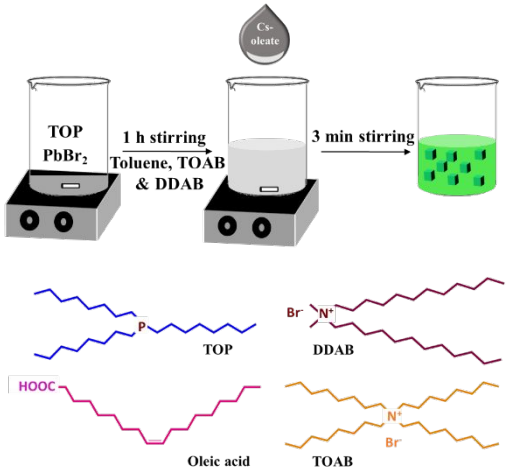

Scheme: Schematic of the quadruple-ligand-assisted room-temperature method for synthesizing $CsPbBr_3$ QDs

The XRD used to understand the crystal structure of both methods synthesized QDs by drop-casting on the glass substrate. Both obtained patterns of well-matched to the cubic phase of $CsPbBr_3$ (ICSD-29073) without the appearance of any other phases (Figure 1). The diffraction peaks of RT-$CsPbBr_3$ QDs appeared at 14.93°, 21.13°, and 30.43°, which assigned as (001), (011), and (002), respectively. HI-$CsPbBr_3$ QDs show 15.01°, 21.24°, and 30.47°, which assigned as (001), (011) and (002). The XRD results in both methods only observe the high intense peak of (00n) because of the preferred orientation phenomenon on the glass substrate.[27, 28]

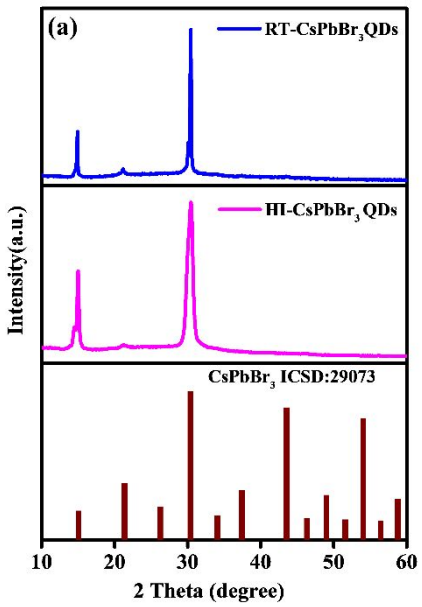

Figure 1. (a) X-ray diffraction pattern (XRD) of RT-$CsPbBr_3$ and HI-$CsPbBr_3$ QDs on glass substrate.

We further study the particle morphology via a high-resolution transmission electron microscope (HRTEM) (Figures 2a and 2b). Both RT-$CsPbBr_3$ and HI-$CsPbBr_3$ QDs exhibit similar cube shape nanocrystal, with an average edge length of 8.13 ± 1.35 and 9.86 ± 1.24 nm, respectively (Figure S1). The "black dots" can be observed on almost every HI-$CsPbBr_3$ QDs, but only a few on the RT-$CsPbBr_3$ QDs. Some reports conclude the formation of black dots on $CsPbX_3$ QDs because of the electron beam irradiation,[29, 30] but Udayabhaskararao *et al.*[31] found these types of black dots in the $CsPbBr_3$ QDs are Pb(0) nanoparticles which form in hot injection method during the growth. Li *et al.*[32] observed surface treatment by ZnX_2(X= Cl, Br & I) remove black dots (PbX_2) from $CsPbX_3$ (X=Cl, Br & I) which subsequently enhances the PLQY. Absorption and PL spectra are shown in Figure 2c. In the absorption spectra, both methods synthesized QDs showed the same first excitation peak, which indicates that their band gaps are nearly the same. This is because of the fact that the bandgap is defined by the Pb 6s-Br 4p hybridized orbitals and the Pb 6p orbitals in the lead halide PQDs.[33] Both RT-$CsPbBr_3$ and HI-$CsPbBr_3$ QDs are excited by 460 nm light and emission observed at 507 and 512 nm, respectively. The blue shift in the emission because of the smaller size of QDs of RT-$CsPbBr_3$ compare to HI-$CsPbBr_3$. The RT-$CsPbBr_3$ QDs performed obvious higher PL intensity compared with HI-$CsPbBr_3$ QDs, which is corresponded to absolute PLQY values of 83% and 45%, respectively. Previously several groups have been published with high PLQY (>85%) but no one discusses the stability issue.[10, 13, 19] To evaluate the stability, both samples are stored at the humidity of 60–70% at 25 ± 5 °C in hexane. PLQY of RT-$CsPbBr_3$ stable at

81% and HI-$CsPbBr_3$ reduce to 41% after 112 days. These results confirm the ligand assisted assembly to improve the PLQY as well as stability which makes it suitable for optoelectronic devices application. Recently Dutta *el al*[34] synthesized $CsPbBr_3$ QDs using hot injection method at 220-260 °C under the presence oleylammonium halide salt and achieved near-unity quantum yields. Further, we used Fourier transform infrared spectroscopy (FTIR) to obtain information about the different types of ligands on the surface RT-$CsPbBr_3$ and HI-$CsPbBr_3$ QDs in Figure S2. Both methods synthesized QDs show peak at ~723, ~2922 and ~2853 cm^{-1} presence of -(CH_2)n, -CH_2, and CH_3 group

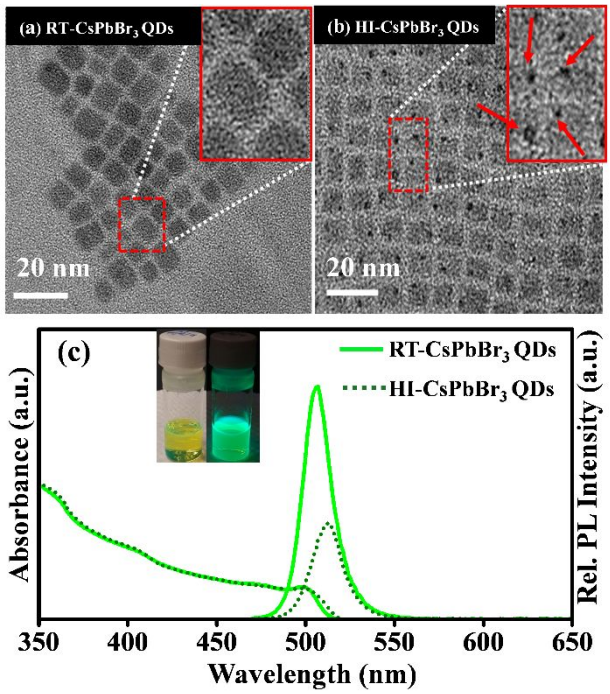

Figure 2: Transmission electron microscope images of (a) RT-$CsPbBr_3$ and (b) HI-$CsPbBr_3$ QDs; insets: the zoomed image of selected area. (c) Absorption and photoluminescence spectra of RT-$CsPbBr_3$ and HI-$CsPbBr_3$ QDs; inserts: the images of RT-$CsPBBr_3$ QDs under visible and UV light.

respectively of oleic acid, because of oleylamine, DDAB, TOAB, and TOP.[35] Additional RT-$CsPbBr_3$ QDs show peaks at 1144 cm^{-1} because of C-P stretching peak of TOP.[36] These all results confirm the surface passivation by different types of ligands on both QDs.

XPS has been used to analyze the different oxidation states and coordination environment of Pb 4*f* and Br 3*d* (Figure 3a and 3b), respectively. We observed the 0.3 eV of the shift in higher binding energy for both RT-$CsPbBr_3$ and HI-$CsPbBr_3$ QDs relatively. RT-$CsPbBr_3$ QDs only showed one set of intensity peaks at 138.3 eV ($4f_{7/2}$) and 143.2 eV ($4f_{5/2}$), which correspond to inner Pb ions. While we found two sets of peaks in Pb 4*f* spectrum of HI-$CsPbBr_3$ QDs. One set of intensity peaks at 138.6 eV ($4f_{7/2}$) and 143.5 eV ($4f_{5/2}$) showed because of inner Pb ions. Another set of shoulder peaks position at 137.5 eV ($4f_{7/2}$) and 142.4 eV ($4f_{5/2}$), indicated the presence of surface Pb ions. Woo *et al*.[37] observe the higher binding energy and lower binding energy because of Pb-Br and Pb-oleate on the surface nanocrystals respectively. Yang *et al*.[22] found the appearance of shoulder peaks due to the surface Pb ions which resultantly create halide defects on the surface of QDs. Zhang *et al*.[10] also detect shoulder peak in bulk $CsPbBr_3$ and lacking in LARP synthesized PQDs. These results suggest the presence of Pb-O on the surface of HI-$CsPbBr_3$ QDs and RT-$CsPbBr_3$ QDs only have Pb-Br chemical environments. We further examined the comparative Br 3*d* spectra for PQDs to understand halide defects on the surface. The spectrum of RT-$CsPbBr_3$ QDs consist of two peaks at 68.3 and 69.3 eV, and that of HI-$CsPbBr_3$ can be fitted at 68.6 and 69.6 eV. According to the previous report,[10] for Br 3*d* in $CsPbBr_3$ QDs, the peak at low binding energy (67.7 eV) present inner Br ions, and the high energy one (68.7 eV) exhibit the surface Br ions. The surface to inner bromide peak ratios of RT-$CsPbBr_3$ and HI-$CsPbBr_3$ QDs are 0.66 and 0.26, respectively. The results of Pb 4*f* and Br 3*d* indicates the completeness of Pb-Br octahedron in RT-$CsPbBr_3$ QDs and the existence of surface Pb ions in HI-$CsPbBr_3$ QDs create halide defects.

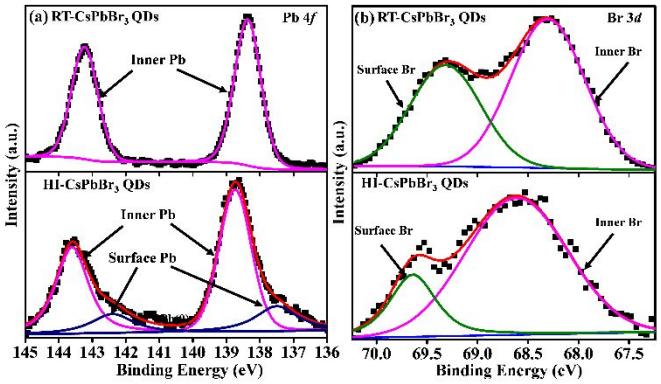

Figure 3. X-ray photoelectron spectroscopy (XPS) spectra of a) Pb 4*f* and b) Br 3*d* for RT-$CsPbBr_3$ and HI-$CsPbBr_3$ QDs.

The surface Pb and Br ions strongly influence the trion formation in PQDs. Figure 4 shows the TA signals monitored at approximately 500 nm for RT-$CsPbBr_3$ and HI-$CsPbBr_3$ QDs under 400 nm excitation. The fast-decay component within 0.5 ns in RT-$CsPbBr_3$ QDs (Figure 4a) is significantly suppressed compared with that in HI-$CsPbBr_3$ QDs (Figure 4b). This fast-decay component is composed of biexcitons and trions. We analyzed the generation ratio of excitons, trions, and biexcitons by using the fitting procedure with a triple exponential decay function.[38] The generation ratio is shown in (Figure 4c and 4d) as a function of the excitation fluence for RT-$CsPbBr_3$ and HI-$CsPbBr_3$ QDs. All components increase with the excitation fluence, and the saturation tendency of excitons (A_X) indicates that the excitation fluence is close to the strong excitation regime where almost all QDs absorb one or more photons. The important difference between RT-$CsPbBr_3$ and HI-$CsPbBr_3$ QDs is the number of trions (A_X*). Here, the amounts of trions should be discussed in terms of A_{X*}/A_X because the QD density difference of RT-$CsPbBr_3$ and HI-$CsPbBr_3$ QDs is normalized by A_X. The trion formation ratio A_{X*}/A_X in RT-$CsPbBr_3$ QDs is significantly suppressed compared with that of HI-$CsPbBr_3$ QDs. This suppression is confirmed by TRPL measurements (Figure

S3). The fast-decay PL component due to trions clearly appears in the HI-$CsPbBr_3$ QDs. The PL data are consistent well with the TA data. These findings indicate that the PLQY enhancement in RT-$CsPbBr_3$ QDs is caused by the suppression of trion formation. In single-dot spectroscopy, we measured the optical spectra of 71 single PQDs for RT-$CsPbBr_3$ and 43 single PQDs for HI-$CsPbBr_3$.The previous study[39] reported that the PL intermittency of the single PQD can be classified into blinking or flickering types. Figures S4 and S5 show the typical blinking and flickering behaviours in RT-$CsPbBr_3$ and HI-$CsPbBr_3$, respectively. The blinking NC shows the binary on–off switching of the PL intensity, while the flickering NC shows the gradual undulation of the PL intensity. The flickering is caused by the presence of surface traps.[22] The surface traps are also related to the trion formation.[22] The ratios of blinking and flickering are 61:10 and 32:11 for RT-$CsPbBr_3$ and HI-$CsPbBr_3$ QDs. This fact means that the HI-$CsPbBr_3$ sample includes many QDs with surface traps compared to the RT-$CsPbBr_3$ sample. The trion formation is suppressed by the absence of surface Pb ions and the high bromide surface in RT-$CsPbBr_3$ QDs. These optical results are consistent with the analysis of XPS characterization.

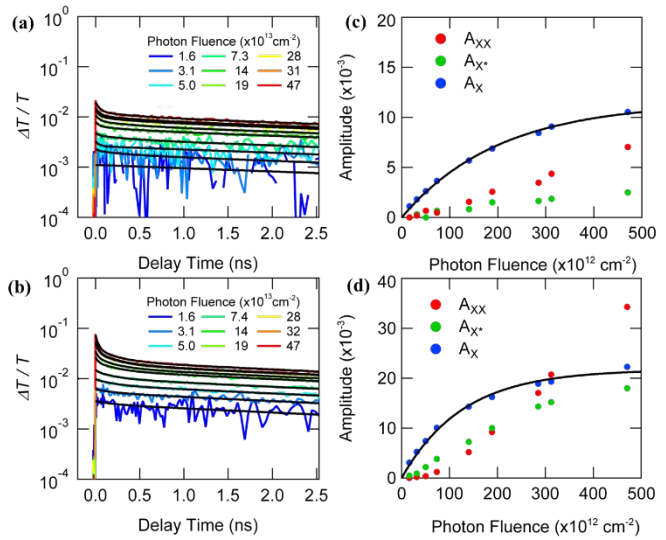

Figure 4. Transient absorption signals of RT-$CsPbBr_3$ and HI-$CsPbBr_3$ QDs. Decay profiles for (a) RT-$CsPbBr_3$ and (b) HI-$CsPbBr_3$ QDs at different excitation photon fluences. Amplitudes of excitons (A_X), trions (A_{X^*}), and biexcitons (A_{XX}) for (c) RT-$CsPbBr_3$ and (d) HI-$CsPbBr_3$ QDs as a function of the excitation photon fluence.

Both method-synthesized $CsPbBr_3$ QDs are mixed with K_2SiF_6: Mn^{4+} (KSF) in silicone resin and then dropped on the blue-chip for LED packaging. The emission spectra of LED devices based on RT-$CsPbBr_3$ and HI-$CsPbBr_3$ QDs are shown in Figure 5a. The green emission observed from RT-$CsPbBr_3$ and HI-$CsPbBr_3$ QDs is obtained at 509 and 521 nm, respectively. Compared with PL spectra, the green emission of HI-$CsPbBr_3$ QDs in LED device red-shifted 9 nm while that of RT-$CsPbBr_3$ QDs only red-shifted 2 nm, which is due to the aggregation in HI-$CsPbBr_3$ QDs on the blue-chip with KSF. The color coordinates of the LEDs based on both method-synthesizing PQDs are optimized at (0.24, 0.28) in CIE 1931, which is a suitable location for backlight display.[40] The RT-$CsPbBr_3$ QDs based white LED exhibited a wide color-gamut of 124% National Television System Committee (NTSC) standard area shown in Figure 5b. The RT-$CsPbBr_3$ QDs based LED also performed a higher luminous efficacy of 62 lm/W than that of HI-$CsPbBr_3$ QDs base one (30 lm/W). These results of luminous efficacy consistent with the PLQY for both RT-$CsPbBr_3$ and HI-$CsPbBr_3$ QDs. This enhanced performance of RT-$CsPbBr_3$ QDs based LED device more suitable for backlight application.

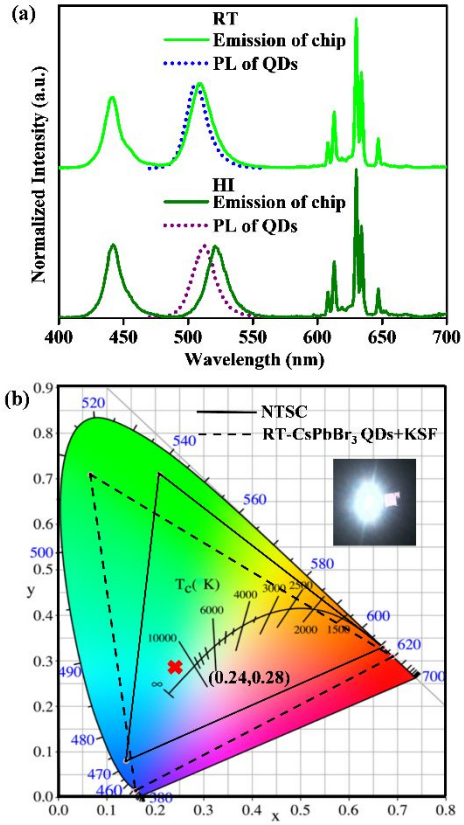

Figure 5. (a) Emission spectra of white LED devices fabricated by RT-$CsPbBr_3$ or HI-$CsPbBr_3$ QDs with K_2SiF_6: Mn^{4+}; The dash lines are the PL spectra of each PQDs sample for comparison. (b) The color gamut of RT-$CsPbBr_3$ QDs based LED (124%) (inset: the working-status image).

Conclusion

In summary, we demonstrated a complete room temperature approach for synthesizing high-efficiency $CsPbBr_3$ quantum dots without inert gas protection. TOP, TOAB, and DDAB are applied to improve the dissolving ability of $PbBr_2$ in toluene as well as to enhance the surface passivation during nucleation. Room temperature synthesized $CsPbBr_3$ exhibit cubic phase and nano-cube shape morphology with PLQY up to 83%. The PLQY of RT-$CsPbBr_3$ QDs is stable and only reduces to 81% after 112 days. The XPS spectra confirmed the absence of Pb ions on the surface and Br-rich in RT-$CsPbBr_3$ compared to HI-$CsPbBr_3$ QDs. The TA study revealed the trion suppression in RT-$CsPbBr_3$ reduced the trap states, which is consistent with the absence of surface Pb ions signal in XPS spectra. The LED device based on RT-$CsPbBr_3$ QDs and KSF performed a wide color gamut of 124% NTSC with high luminous efficacy of 62 lm/W.

Acknowledgments

This work is financially supported by the "Advanced Research Center of Green Materials Science and Technology" from The Featured Area Research Center Program within the framework of the Higher Education Sprout Project by the Ministry of Education (107L9006) and the Ministry of Science and Technology in Taiwan (MOST 107-2113-M-002-008-MY3 & 107-3017-F-002-001). We also thankful to the Japan Society for the Promotion of Science (JSPS) Core-to-Core Program (A) Advanced Research Networks for the support. Part of this work, which was conducted in Kyoto, was supported by JST-CREST, Japan (JPMJCR16N3).

Notes and references

1. J. Kang and L. W. Wang, *J. Phys. Chem. Lett.*, 2017, **8**, 489-493.
2. A. Swarnkar, R. Chulliyil, V. K. Ravi, M. Irfanullah, A. Chowdhury and A. Nag, *Angew. Chem.*, 2015, **54**, 15424-15428.
3. A. Swarnkar, A. R. Marshall, E. M. Sanehira, B. D. Chernomordik, D. T. Moore, J. A. Christians, T. Chakrabarti and J. M. Luther, *Science*, 2016, **354**, 92-95.
4. J. Song, J. Li, X. Li, L. Xu, Y. Dong and H. Zeng, *Adv. Mater.*, 2015, **27**, 7162-7167.
5. Y. H. Song, J. S. Yoo, B. K. Kang, S. H. Choi, E. K. Ji, H. S. Jung and D. H. Yoon, *Nanoscale*, 2016, **8**, 19523-19526.
6. L. Dou, Y. Yang, J. You, Z. Hong, W. H. Chang, G. Li and Y. Yang, *Nat. Comm.*, 2014, **5**, 5404.
7. K. Chen, Y. Wang, J. Liu, J. Kang, Y. Ge, W. Huang, Z. Lin, Z. Guo, Y. Zhang and H. Zhang, *Nanoscale*, 2019, **11**, 16852-16859.
8. Y. Wang, X. Li, J. Song, L. Xiao, H. Zeng and H. Sun, *Adv. Mater.*, 2015, **27**, 7101-7108.
9. L. Protesescu, S. Yakunin, M. I. Bodnarchuk, F. Krieg, R. Caputo, C. H. Hendon, R. X. Yang, A. Walsh and M. V. Kovalenko, *Nano Lett.*, 2015, **15**, 3692-3696.
10. F. Zhang, H. Zhong, C. Chen, X. G. Wu, X. Hu, H. Huang, J. Han, B. Zou and Y. Dong, *ACS Nano*, 2015, **9**, 4533-4542.
11. A. D. Jodlowski, A. Yépez, R. Luque, L. Camacho and G. de Miguel, *Angew. Chem., Int. Ed.*, 2016, **55**, 14972-14977.
12. T. Ahmed, S. Seth and A. Samanta, *Chem. Mater.*, 2018, **30**, 3633-3637.
13. J. Song, J. Li, L. Xu, J. Li, F. Zhang, B. Han, Q. Shan and H. Zeng, *Adv. Mater.*, 2018, **30**, 1800764.
14. C. Zhang, B. Wang, Q. Wan, L. Kong, W. Zheng, Z. Li and L. Li, *Nanoscale*, 2019, **11**, 2602-2607.
15. T. Xuan, X. Yang, S. Lou, J. Huang, Y. Liu, J. Yu, H. Li, K. L. Wong, C. Wang and J. Wang, *Nanoscale*, 2017, **9**, 15286-15290.
16. F. Zhang, Z. F. Shi, Z. Z. Ma, Y. Li, S. Li, D. Wu, T.-T. Xu, X.-J. Li, C. X. Shan and G. T. Du, *Nanoscale*, 2018, **10**, 20131-20139.
17. H. C. Wang, W. Wang, A. C. Tang, H. Y. Tsai, Z. Bao, T. Ihara, N. Yarita, H. Tahara, Y. Kanemitsu, S. Chen and R. S. Liu, *Angew. Chem., Int. Ed.*, 2017, **56**, 13650-13654.
18. J. S. Yao, J. Ge, B. N. Han, K. H. Wang, H. B. Yao, H. L. Yu, J. H. Li, B. S. Zhu, J. Z. Song, C. Chen, Q. Zhang, H. B. Zeng, Y. Luo and S. H. Yu, *J. Am. Chem. Soc.*, 2018, **140**, 3626-3634.
19. X. Li, Y. Wu, S. Zhang, B. Cai, Y. Gu, J. Song and H. Zeng, *Adv. Funct. Mater.*, 2016, **26**, 2435-2445.
20. Y. H. Kim, G. H. Lee, Y. T. Kim, C. Wolf, H. J. Yun, W. Kwon, C. G. Park and T. W. Lee, *Nano Energy*, 2017, **38**, 51-58.
21. S. Wei, Y. Yang, X. Kang, L. Wang, L. Huang and D. Pan, *Inorg. Chem.*, 2017, **56**, 2596-2601.
22. D. Yang, X. Li, Y. Wu, C. Wei, Z. Qin, C. Zhang, Z. Sun, Y. Li, Y. Wang and H. Zeng, *Adv. Optical Mater.*, 2019, **7**, 1900276.
23. S. D. Stranks, V. M. Burlakov, T. Leijtens, J. M. Ball, A. Goriely and H. J. Snaith, *Phys. Rev. Applied*, 2014, **2**, 034007.
24. B. A. Koscher, J. K. Swabeck, N. D. Bronstein and A. P. Alivisatos, *J. Am. Chem. Soc.*, 2017, **139**, 6566-6569.
25. S. Nakahara, H. Tahara, G. Yumoto, T. Kawawaki, M. Saruyama, R. Sato, T. Teranishi and Y. Kanemitsu, *J. Phys. Chem. C*, 2018, **122**, 22188-22193.
26. N. Yarita, T. Aharen, H. Tahara, M. Saruyama, T. Kawawaki, R. Sato, T. Teranishi and Y. Kanemitsu, *Phys. Rev. Mater.*, 2018, **2**, 116003.
27. S. Chakrabarti, D. Ganguli and S. Chaudhuri, *Mater. Lett.*, 2004, **58**, 3952-3957.
28. Y. Dong, Y. Gu, Y. Zou, J. Song, L. Xu, J. Li, J. Xue, X. Li and H. Zeng, *Small*, 2016, **12**, 5622-5632.
29. W. Liu, J. Zheng, M. Shang, Z. Fang, K. C. Chou, W. Yang, X. Hou and T. Wu, *J. Materi. Chem. A*, 2019, **7**, 10912-10917.
30. J. D. McGettrick, K. Hooper, A. Pockett, J. Baker, J. Troughton, M. Carnie and T. Watson, *Mater. Lett.*, 2019, **251**, 98-101.
31. T. Udayabhaskararao, M. Kazes, L. Houben, H. Lin and D. Oron, *Chem. Mater.*, 2017, **29**, 1302-1308.
32. F. Li, Y. Liu, H. Wang, Q. Zhan, Q. Liu and Z. Xia, *Chem. Mater.*, 2018, **30**, 8546-8554.
33. M. Mittal, A. Jana, S. Sarkar, P. Mahadevan and S. Sapra, *J. Phy. Chem. Lett.*, 2016, **7**, 3270-3277.
34. A. Dutta, R. K. Behera, P. Pal, S. Baitalik and N. Pradhan, *Angew. Chem., Int. Ed.*, 2019, **58**, 5552-5556.
35. X. Lu, B. A. Korgel and K. P. Johnston, *Chem.Mater.*, 2005, **17**, 6479-6485.
36. H. Guo, Y. Chen, H. Ping, J. Jin and D. L. Peng, *Nanoscale*, 2013, **5**, 2394-2402.
37. J. Y. Woo, Y. Kim, J. Bae, T. G. Kim, J. W. Kim, D. C. Lee and S. Jeong, *Chem. Mater.*, 2017, **29**, 7088-7092.
38. N. Yarita, H. Tahara, T. Ihara, T. Kawawaki, R. Sato, M. Saruyama, T. Teranishi and Y. Kanemitsu, *J. Phys. Chem. Lett.*, 2017, **8**, 1413-1418.
39. N. Yarita, H. Tahara, M. Saruyama, T. Kawawaki, R. Sato, T. Teranishi and Y. Kanemitsu, *J. Phys. Chem. Lett.*, 2017, **8**, 6041-6047.
40. H. C. Wang, S. Y. Lin, A. C. Tang, B. P. Singh, H. C. Tong, C. Y. Chen, Y. C. Lee, T. L. Tsai and R. S. Liu, *Angew. Chem., Int. Ed.*, 2016, **55**, 7924-7929.

Table of Content: